

Development of new finite elements for fatigue life prediction in structural components

Wasim Tarar, Onome Scott-Emuakpor and *M.-H. Herman Shen

*Department of Mechanical and Aerospace Engineering, The Ohio State University,
2036 Neil Ave. Bolz Hall, Room 328, Columbus, OH 43210, USA*

(Received November 7, 2007, Accepted February 24, 2010)

Abstract. An energy-based fatigue life prediction framework was previously developed by the authors for prediction of axial and bending fatigue life at various stress ratios. The framework for the prediction of fatigue life via energy analysis was based on a new constitutive law, which states the following: the amount of energy required to fracture a material is constant. In this study, the energy expressions that construct the new constitutive law are integrated into minimum potential energy formulation to develop new finite elements for uniaxial and bending fatigue life prediction. The comparison of finite element method (FEM) results to existing experimental fatigue data, verifies the new finite elements for fatigue life prediction. The final output of this finite element analysis is in the form of number of cycles to failure for each element in ascending or descending order. Therefore, the new finite element framework can provide the number of cycles to failure for each element in structural components. The performance of the fatigue finite elements is demonstrated by the fatigue life predictions from Al6061-T6 aluminum and Ti-6Al-4V. Results are compared with experimental results and analytical predictions.

Keywords: bending; cycles; fatigue; finite element analysis; structures; uniaxial.

1. Introduction

The modern structural components, like gas turbine engine blades, are designed to be failure free and last their life; however, failure does occur and is commonly linked to fatigue. High cycle fatigue (HCF) is the main cause of failure in gas turbine engines (Nicholas 1999). Different design tools have been developed to analyze this issue. The most commonly used such tool is a stress versus cycles plot, or S-N curve. These curves provide fatigue strength with respect to time to failure. Other common tools for predicting fatigue properties are the Goodman diagram and the advanced Goodman diagrams (Goodman 1899), which are the popular choices for a failure-free aircraft engine design criterion. In order for designers to make an accurate assessment, the equivalent stress is calculated according to the cyclic loading conditions and compare to S-N curve or Goodman diagram to obtain the number of cycles to failure. This has led to search for a more realistic method for design comparison than the existing uniaxial design tools, which begins by observing the association between material failure/fracture and the energy dissipated during the process.

*Corresponding author, Professor, E-mail: shen.1@osu.edu

Scientists and engineers have tried since 1940s to relate energy conversion to fatigue life prediction of the material. These attempts initially resulted in minimal success (Feltner and Morrow 1960). The hypothesis used in this type of research implies: under cyclic loading, there exists a critical energy value for which failure occurs (Enomoto 1955). The continued research in this area later justified this hypothesis by displaying agreement between the theoretical and the experimental results on S-N curve. Further investigation of the assumption made in (Enomoto 1955) led to the introduction of a more sufficient correlation between the fatigue life of a material and the strain energy dissipation during the process (Feltner and Morrow 1960, Stowell 1966). It is now understood that the strain energy required to fracture a material, monotonically, is the same as the strain energy during a cyclic fatigue procedure, thus indicating that the critical energy value for each material is the monotonic strain energy. Based on this constitutive law, an improved energy-based frame-work has been developed by the researchers to allow one to systematically determine fatigue life based on the amount of energy loss per fatigue cycle (Scott-Emuakpor *et al.* 2007, Scott-Emuakpor 2007). The new constitutive law is based on the monotonic and cyclic stress-strain representation expressed by the following equations

$$\varepsilon = \frac{\sigma}{E} + \varepsilon_o \sinh\left(\frac{\sigma}{\sigma_o}\right) \quad (1)$$

$$\varepsilon = \frac{\sigma_{PP}}{E} + \frac{1}{C} \sinh\left(\frac{\sigma_{PP}}{\sigma_c}\right) \quad (2)$$

Where the parameters displayed are defined as follows: σ is the value for stress at the surface of the specimen (in the bending case, max stress), ε is the strain corresponding to the stress σ , σ_{pp} is the peak to peak stress (2σ when stress ratio is -1.0), E is the modulus of elasticity, and the variables σ_c , σ_o , ε_o , and C are curve fit parameters. The details about this constitutive law, the curve fit parameters, material constants and the experimental procedure adopted for acquiring these constants are explained in (Scott-Emuakpor *et al.* 2007, George *et al.* 2004, George *et al.* 2005, George *et al.* 2006). These equations are used to obtain the total fracture energy and the energy dissipated per cycle. Therefore, the equations can be applied to the constitutive law to obtain the number of cycles to failure.

As stated earlier, the conventional approach to fatigue life prediction is based on S-N curve data, Goodman diagram or modified Goodman diagram. For example, a traditional HCF turbine blading system design procedure is shown schematically in Fig. 1. This design process usually consists of a structural dynamics analysis to determine natural frequencies and mode shapes at certain operating speed ranges and a stress analysis using a finite element based tool such as MSC/NASTRAN and ANSYS (Mackaldener and Olsson 2001, Sumi *et al.* 2005, Salvini *et al.* 1997, Fermér and Svensson 2001) to calculate the dynamic stress distribution for identifying the maximum vibratory stress location or area under a series of given excitations. Once the maximum stresses for each vibration mode are determined, high cycle fatigue assessment can be achieved by measuring the margin between the maximum vibratory stress and the material fatigue capability which is a straight line drawn between the mean ultimate strength at zero vibratory stress and mean fatigue strength at 10^7 cycles (or infinite life). A typical Goodman diagram for the titanium alloy Ti-6Al-4V is shown in Fig. 2 (Nicholas and Maxwell 2003), usually constructed using uniaxial fatigue data.

The new constitutive law based on fatigue energy dissipation mechanism, developed by the authors (Scott-Emuakpor *et al.* 2007, Scott-Emuakpor 2007), provides an opportunity to develop

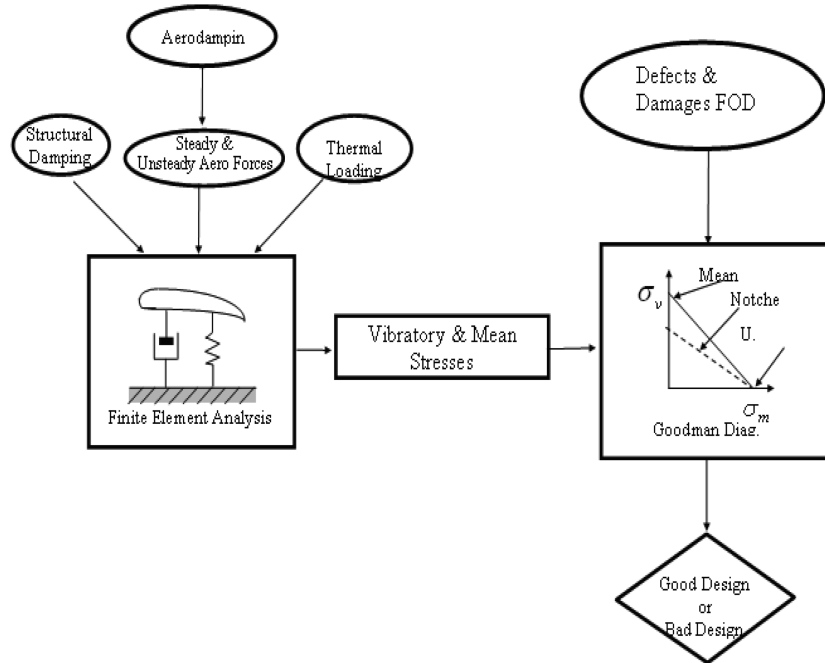


Fig. 1 Conventional finite element analysis approach to fatigue life prediction

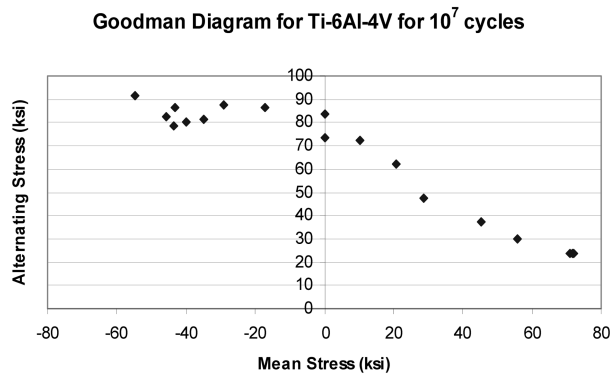


Fig. 2 Typical Goodman (or Haigh) diagram for Ti-6Al-4V for 10^7 cycles (Nicholas and Maxwell 2003)

new finite elements for fatigue life analysis without accomplishing fatigue strength/life assessment through comparison with Goodman diagram or inbuilt S-N data. This research uses the new constitutive law to derive new finite elements for fatigue life prediction for uniaxial and bending loads.

Though the conventional finite element fatigue analysis and design tools for fatigue life prediction make the process easier for designer, however, the process does not incorporate fatigue mechanism (Papanikos *et al.* 2003) and can not characterize the fatigue strength without using Goodman design diagram (LMS Engineering Innovations: <http://www.lmsintl.com>, Desktop Engineering (DE): <http://>

www.deskeng.com, MSC Software: <http://www.mscsoftware.com>). The new finite elements developed in this research are based on a fatigue constitutive law; therefore, the analysis with these elements directly incorporates the fatiguing process in fatigue life prediction. This very fact establishes a difference of these new finite element developments from the existing finite element fatigue analysis techniques. Due to the discrete nature of finite element method, the finite element analysis can provide the number of cycles for each element at different location in the structure experiencing different loads. Furthermore, the most research in the area of fatigue using finite element analysis, involves fatigue crack growth and propagation (Lee and Song 2005, Park *et al.* 1997, Papanikos and Meguid 1994, Ritchie *et al.* 1987, Beretta and Sala 2005, Shang and Barkey 2006), whereas this new finite element predicts the fatigue crack initiation.

In order to derive new finite elements, the constitutive law for fatigue (Scott-Emuakpor *et al.* 2007, Scott-Emuakpor 2007) is integrated into minimum potential energy formulation and new stiffness matrices (K-matrices) for uniaxial and bending fatigue are developed. Due to non-linear nature of the constitutive law, the resulting K-matrices require a non-linear finite element analysis approach. Newton-Raphson iteration method is used for numerical computation to handle the non-linearity. The new K-matrices are capable of simulating the fatigue analysis based on constitutive law and Eqs. (1) and (2). For validation of the finite elements, a monotonic loading analysis on a 1-D rod is performed. The comparison of resulting displacements for monotonic loading is made with the analytical solution (Eq. (1)) as well as experimental results to validate the new K-matrix. Once the K-matrix is validated, the same displacement computation procedure is applied to the cyclic loading case. Furthermore, strain energy is acquired by evaluating the behavior of the respective load-displacement relation of the monotonic and cyclic loading processes. The same procedure is applied to the bending fatigue life prediction using the new bending fatigue finite element (New K-Matrix).

The new finite elements can be applied to a structure made of any material as long as the parameters for the material being used are available. The FEM fatigue prediction procedures developed in this research are performed for Al6061-T6 (both uniaxial and bending) and Ti6Al-4V (uniaxial load only) and the comparison is made with the experimental data and analytical solution from reference (Scott-Emuakpor *et al.* 2007). These results and procedures will be discussed at length in the following sections of the manuscript. Analysis is also performed for a loading condition with mean stress effect. The results from this analysis are also compared to the experimental data and analytical solution.

2. Brief review of previously acquired experimental results

Experimental fatigue results have been acquired for both Al6061-T6 and Ti6Al-4V (Scott-Emuakpor *et al.* 2007). Axial results were acquired from a conventional MTS servo-hydraulic machine. The machine was operated at a frequency of 40 Hz, thus requiring 7 hours to accumulate 10^6 cycles. The axially loaded fatigue results from this machine range approximately from 10^4 to 10^6 for both materials.

The bending data is acquired using vibration based methodology (George *et al.* 2004). The thought behind the vibration-based methodology is supplying a dynamic base excitation to a specimen at a specified high resonant frequency, between 1200-1600 Hz, showing bending behavior. This testing method provides a significantly faster means for acquiring 10^6 cycles (between 10 and 14 minutes), therefore making it a more efficient means for acquiring HCF.

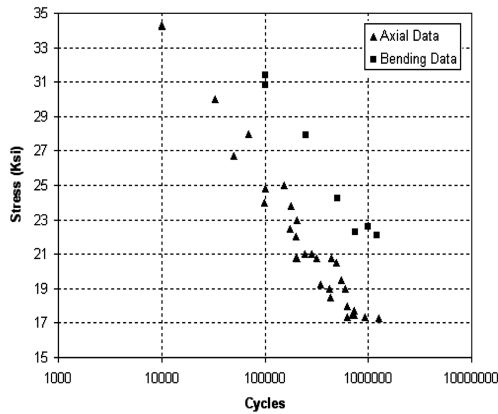


Fig. 3 S-N Data – Al6061-T6 (Scott-Emuakpor *et al.* 2007)

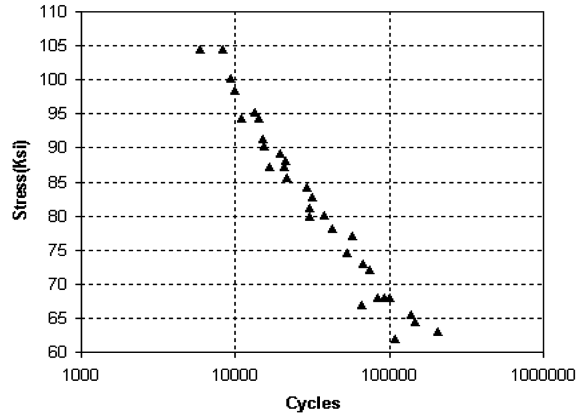


Fig. 4 S-N Data – Ti6Al-4V axial data (Scott-Emuakpor *et al.* 2007)

Experimental fatigue results for Al6061-T6 and Ti6Al-4V are shown in Figs. 3 and 4 respectively (Scott-Emuakpor *et al.* 2007). These results display an acceptable scatter for failure ranging from 10^4 to roughly over 10^6 cycles. Therefore, the behavior of fatigue as applied load increases or decreases can easily be characterized visually.

3. Finite element procedures

The respective expression of Eqs. (1) and (2) consists of two parts, the linear elastic and the non-linear plastic. The main challenge in this research is to handle the both parts correctly and develop a procedure which provides a best match with analytical and experimental results. The elastic and plastic parts of Eqs. (1) and (2) are written separately in Eqs. (3) to (6) respectively: where the subscripts *em* and *pm* designate the elastic and plastic cases for monotonic loading, and the subscripts *ec* and *pc* designate the elastic and plastic cases for cyclic loading.

$$\epsilon_{em} = \frac{\sigma}{E} \tag{3}$$

$$\epsilon_{pm} = \epsilon_o \sinh\left(\frac{\sigma}{\sigma_o}\right) \tag{4}$$

$$\epsilon_{ec} = \frac{\sigma_{PP}}{E} \tag{5}$$

$$\epsilon_{pc} = \frac{1}{C} \sinh\left(\frac{\sigma_{PP}}{\sigma_c}\right) \tag{6}$$

Eqs. (7) to (10) give the corresponding stress equations to these provided strain expressions; where σ_{ec} and σ_{pc} are the corresponding peak-to-peak stresses for cyclic loading case. These equations are integrated into minimum potential energy formulation to develop new K-matrices.

$$\sigma_{em} = E\varepsilon \quad (7)$$

$$\sigma_{pm} = \sigma_o \sinh^{-1}\left(\frac{\varepsilon_p}{\varepsilon_o}\right) \quad (8)$$

$$\sigma_{ec} = E\varepsilon \quad (9)$$

$$\sigma_{pc} = \sigma_c \sinh^{-1}(C\varepsilon_p) \quad (10)$$

The procedure for integration of constitutive law into minimum potential energy formulation is included in the following two sections for uniaxial and bending loads respectively.

3.1 Finite element procedures for uniaxial load (rod element)

Integration of elastic case into potential energy formulation is a classical finite element problem and is already available in literature (Reddy 1984). Integration of Eqs. (8) and (10) into Eq. (11) provides new K-matrix for the plastic part of the constitutive law (Eqs. (1) and (2)) for uniaxial fatigue.

$$\Pi = \int_0^L \frac{1}{2} \sigma \varepsilon dV - \int u f dV - \int u T dx - \sum u_i P_i \quad (11)$$

Where Π is the minimum potential energy, σ is the stress tensor, ε is the strain vector, u is the displacement, f is the body force, T is the traction force, P_i is the point load. V is the volume and x denotes the length of the element.

The resulting K-matrices for monotonic case with axial loading based on Eq. (1) are shown below.

$$K_{em-A} = \frac{AE}{L} \begin{bmatrix} +1 & -1 \\ -1 & +1 \end{bmatrix} \quad (12)$$

$$K_{pm-A} = \sigma_o A \begin{bmatrix} -\frac{1}{d_1} \sinh^{-1}\left(\frac{-d_1/L}{\varepsilon_o}\right) & +\frac{1}{d_1} \sinh^{-1}\left(\frac{-d_1/L}{\varepsilon_o}\right) \\ -\frac{1}{d_2} \sinh^{-1}\left(\frac{+d_2/L}{\varepsilon_o}\right) & +\frac{1}{d_2} \sinh^{-1}\left(\frac{+d_2/L}{\varepsilon_o}\right) \end{bmatrix} \quad (13)$$

A is the area, L is the length of the element and d is the nodal displacement. The similar types of matrices are developed for cyclic load according to Eq. (2). The parameters σ_o changes to σ_c , ε_o changes to C and the applied stress σ changes to peak to peak stress σ_{pp} . The resulting K-matrices are shown in Eqs. (14) and (15).

$$K_{ec} = \frac{AE}{L} \begin{bmatrix} +1 & -1 \\ -1 & +1 \end{bmatrix} \quad (14)$$

$$K_{pc} = \sigma_c A \begin{bmatrix} -\frac{1}{d_1} \sinh^{-1}(-Cd_1/L) & +\frac{1}{d_1} \sinh^{-1}(-Cd_1/L) \\ -\frac{1}{d_2} \sinh^{-1}(+Cd_2/L) & +\frac{1}{d_2} \sinh^{-1}(+Cd_2/L) \end{bmatrix} \quad (15)$$

As is evident from Eqs. (13) and (15), a non-linearity appears in the expression. This non-linearity is due to an existing displacement parameter in the resulting K-matrices. To account for the non-linear behavior, the Newton-Raphson iteration method is applied to the analysis (Reddy 2004, Masud and Khurram 2004, Khurram and Masud 2006).

Application of energy balance leads to the classical representation of load, F , versus displacement, d , shown by Eq. (16). Therefore, based on a known applied load, the K-matrices can be used in Eq. (16) to determine the nodal displacements. Results from the nodal displacements and corresponding loads are used to obtain a cyclic and monotonic stress-strain relation. Therefore, the capability exists to apply the stress-strain results to the constitutive law and the number of cycles to failure can be calculated.

$$[K]\{d\} = \{F\} \quad (16)$$

3.2 Finite element procedures for bending load (beam element)

The finite element (new K-Matrix) for bending fatigue is developed by integration of new constitutive law into bending energy formulation. Bending stress is given by the Eq. (17).

$$\sigma = -\frac{My}{I} \quad (17)$$

Where M is the bending moment, y is the distance from the neutral axis and I is the moment of inertia. The development of K-matrix for elastic bending is a classical finite element problem and is available in the literature (Reddy 1984). The equation for plastic bending derived from Eq. (10) is given by the following expression.

$$M = \int y \sigma dA = \int \frac{I \sigma_o}{y} \sinh^{-1}\left(\frac{\varepsilon_p}{\varepsilon_o}\right) \quad (18)$$

The potential energy of the beam is given by

$$\Pi = \int_0^L \frac{1}{2} \sigma \varepsilon dV - \int_0^L p v dx - \sum_m P_m v_m - \sum_m M_k v_k' \quad (19)$$

Where p is the distributed load per unit length, P_m is the point load at point m , M_k is the moment of the couple applied at point k , v_m is the deflection at point m and v_k' is the slope at point k . Integration of Eqs. (4) and (18) into Eq. (19) provides the K-matrix for non-linear part of the constitutive law for bending loads.

Using the potential energy formulation, the resulting K-matrices for bending loading are shown below in Eqs. (20) and (21). K_{em-B} and K_{pm-B} are the linear elastic and non-linear plastic K-matrices for bending load respectively. l_e represents the length of the beam element.

$$K_{em-B} = \frac{EI}{l_e^3} \begin{bmatrix} 12 & 6l_e & -12 & 6l_e \\ 6l_e & 4l_e^2 & -6l_e & 2l_e^2 \\ -12 & -6l_e & 12 & -6l_e \\ 6l_e & 2l_e^2 & -6l_e & -4l_e^2 \end{bmatrix} \tag{20}$$

$$K_{pm-B} = \frac{2\sigma_o I}{l_e y} \begin{bmatrix} k_{11pm}(d_1) & k_{12pm}(d_1) & k_{13pm}(d_1) & k_{14pm}(d_1) \\ k_{21pm}(d_2) & k_{22pm}(d_2) & k_{23pm}(d_2) & k_{24pm}(d_2) \\ k_{31pm}(d_3) & k_{32pm}(d_3) & k_{33pm}(d_3) & k_{34pm}(d_3) \\ k_{41pm}(d_4) & k_{42pm}(d_4) & k_{43pm}(d_4) & k_{44pm}(d_4) \end{bmatrix} \tag{21}$$

The elements of K_{pm-B} are given in Eqs. (22) and (23)

$$k_{ij-pm} = \frac{0.866}{d_i} \{C_j \sinh^{-1}(A_i d_i) - D_j \sinh^{-1}(B_i d_i)\} \quad \text{for } i = 1, 2, 3, 4 \quad \text{and } j = 1, 3 \tag{22}$$

$$k_{ij-pm} = \frac{l_e}{d_i} \{C_j \sinh^{-1}(A_i d_i) - D_j \sinh^{-1}(B_i d_i)\} \quad \text{for } i = 1, 2, 3, 4 \quad \text{and } j = 2, 4 \tag{23}$$

A_i, B_i, C_j and D_j are given in Table 1.

The similar equations are developed for cyclic bending load according to Eq. (2). The resulting K-matrices are shown in Eqs. (24) and (25).

$$K_{ec-B} = \frac{EI}{l_e^3} \begin{bmatrix} 12 & 6l_e & -12 & 6l_e \\ 6l_e & 4l_e^2 & -6l_e & 2l_e^2 \\ -12 & -6l_e & 12 & -6l_e \\ 6l_e & 2l_e^2 & -6l_e & -4l_e^2 \end{bmatrix} \tag{24}$$

Table 1 Constants for Eqs. (22) and (23)

i	A_i	B_i	C_j	D_j
1	$\frac{3.46y}{\epsilon_o l_e^2}$	$\frac{-3.46y}{\epsilon_o l_e^2}$	1	1
2	$\frac{0.732y}{\epsilon_o l_e}$	$\frac{-2.732y}{\epsilon_o l_e}$	0.183	0.683
3	$\frac{-3.46y}{\epsilon_o l_e^2}$	$\frac{3.46y}{\epsilon_o l_e^2}$	-1	-1
4	$\frac{2.732y}{\epsilon_o l_e}$	$\frac{-0.732y}{\epsilon_o l_e}$	0.683	0.183

$$K_{pc-B} = \frac{2\sigma_c I}{l_e y} \begin{bmatrix} k_{11pc}(d_1) & k_{12pc}(d_1) & k_{13pc}(d_1) & k_{14pc}(d_1) \\ k_{21pc}(d_2) & k_{22pc}(d_2) & k_{23pc}(d_2) & k_{24pc}(d_2) \\ k_{31pc}(d_3) & k_{32pc}(d_3) & k_{33pc}(d_3) & k_{34pc}(d_3) \\ k_{41pc}(d_4) & k_{42pc}(d_4) & k_{43pc}(d_4) & k_{44pc}(d_4) \end{bmatrix} \quad (25)$$

The elements of K_{pc-B} are the same as given in Eqs. (22) and (23) except that the parameters σ_o changes to σ_c , ε_o changes to $1/C$ and the applied stress σ changes to peak to peak stress σ_{pp} .

The matrices in Eqs. (21) and (25) are non-linear due to presence of “ ds ” in the resulting K-matrices. To account for the non-linear behavior, the Newton-Raphson iteration method is applied to the analysis (Reddy 2004, Masud and Khurram 2004, Khurram and Masud 2006).

These K-matrices are used in Eq. (16) to determine the unknown degrees of freedom. The load is applied from 0 to peak to peak. The results are post-processed using classical FEA techniques. The nodal displacement and rotation results can be further used to obtain moment for each element in the structure. This moment is used to calculate the bending energy dissipated per cycle and ultimately the number of cycles to failure for each element.

4. Pre and post processing of data

The procedures presented in this section are primarily for 1-D loads. However, similar pre and post-processing procedures are valid for bending loads.

The computational FEM analysis was tailored to correspond to the experimental procedures for the results in section 2. The related geometric data was acquired from the ASTM standard E466 fatigue dog-bone (coupon) specimen (Scott-Emuakpor *et al.* 2007). This specimen is loaded in axial tension for the monotonic case and tension/compression for cyclic. The monotonic loading produces force vs. displacement data, which is converted to stress-strain relation in the form of Fig. 5. The fatigue analysis is only performed below the yield point. Therefore, this relation is only analyzed up to the point of yielding for the validation of K-Matrix. This analysis is performed for Al6061-T6 and Ti6Al-4V material parameters. The resulting solution is compared with the experimental and analytical results (Eq. (1)). These results are shown in Section 5.

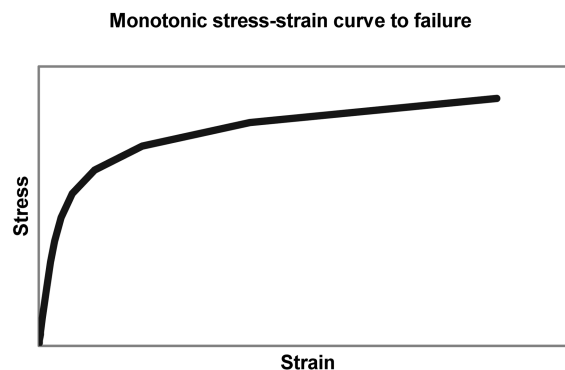


Fig. 5 Monotonic stress-strain relation

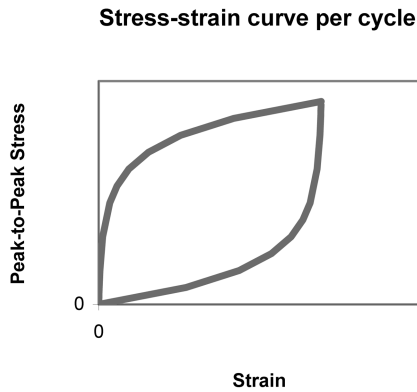


Fig. 6 Hysteresis loop for completely reversible loading

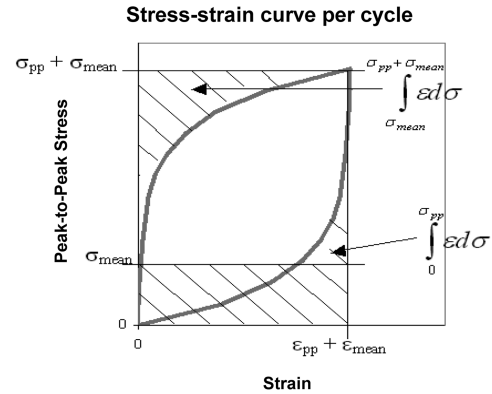


Fig. 7 Hysteresis loop with mean stress effect

The cyclic process is executed by tension/compression loading at a specified level. In other words, fully-reversed loading ranges from $-P$ to $+P$, where P is the parameter representing the specified loading level. This understanding leads to the conclusion that the cyclic stress-strain behavior, which is acquired from the corresponding load-displacement relation, forms the loop shown on the generalized axis of Fig. 6. The stress-strain relation of Fig. 6 is known as a hysteresis loop. The area inside this loop represents the cyclic strain energy density energy for the applied stress level. In order to calculate the number of cycles to failure, the cyclic strain energy acquired from the constitutive law is compared to the monotonic failure strain energy (Scott-Emuakpor *et al.* 2007). This analysis was conducted with Ti6AL-4V as well as Al6061-T6 material parameters. The results were compared with experimental data and the analytical solution (Scott-Emuakpor *et al.* 2007).

Fig. 7 represents the hysteresis loop with the mean stress effect. The figure shows that the calculation of strain energy density for this case is different from completely reversible loading analysis. Due to a larger maximum applied load, the effect of mean stress increases the plastic deformation per cycle for a designated alternating load. Also based on an increase in the minimum applied load, the stress-strain relation no longer is viewed as a closed loop. Therefore, the unshaded area of Fig. 7 represents cyclic strain energy density. This analysis is performed for Al6061-T6 and the results are compared to experimental data and the analytical solution.

As stated earlier, the procedure presented in this section is for 1-D axial loads but is also valid for bending loads. The solution of all unknown degrees of freedoms obtained from FEM analysis is post-processed using the classical FEM techniques (Reddy 1984) to obtain the strain energy dissipated per cycle and finally the number of cycles to failure. Analysis is performed for Al6061-T6 both for completely reversible and means stress effects bending loads. The K-matrix for bending loads is capable of predicting different number of cycles for each element depending upon the different stress level. The results are compared to the experimental and analytical results (Scott-Emuakpor *et al.* 2007).

5. Results and discussion

The following sections present the results and comparisons for axial bending loads respectively.

5.1 1-D axial load analysis

The finite element analysis results and analytical solution are obtained for a 1-D rod in order to compare and validate the results. The dimensions of this rod are provided in (Scott-Emuakpor *et al.* 2007). A set of experimental data from previous research (Scott-Emuakpor *et al.* 2007) is also included in the comparison. Fig. 8 shows the Force vs. Displacement curves for Al6061-T6 with experimental data, analytical solution (Scott-Emuakpor *et al.* 2007) and FEM prediction plotted for comparison. These curves are plotted for a monotonically loaded specimen below the yield point. The FEM prediction compares well with the experimental and analytical results.

Fig. 9 shows the True stress vs. True strain, for FEM prediction and analytical solution (Scott-Emuakpor *et al.* 2007) plotted in comparison to experimental data. The specimen is loaded monotonically below the yield point.

Figs. 8 and 9 show a very good match of FEM prediction to the experimental data and analytical solution, thus, validating the newly developed K-matrix and FEM procedure.

The constitutive law in Eqs. (1) and (2) consists of linear and non-linear parts. The plastic part of Eqs. (1) and (2) induces non-linearity in the results. This non-linearity helps in producing hysteresis loop when dealing with the cyclic loading. As stated earlier, the area enclosed by this hysteresis loop provides the energy loss per cycle.

Though the constitutive law in Eqs. (1) and (2) has the capability to capture the plastic strain but the contribution of this strain to the total strain is very small. This makes the curves in Figs. 8, 9 and 10 almost look linear. In order to display the non-linearity present in the data, results are normalized and are shown in Fig. 10.

Eq. (2) parameters and corresponding K-matrix is used to construct the S-N curve for Al6061-T6 and is shown in Fig. 11 on a semi log scale. Experimental data, analytical solution (Scott-Emuakpor *et al.* 2007) and FEM prediction are plotted on the same graph for comparison. The FEM curve shows a good agreement with experimental data and analytical results (Scott-Emuakpor *et al.* 2007).

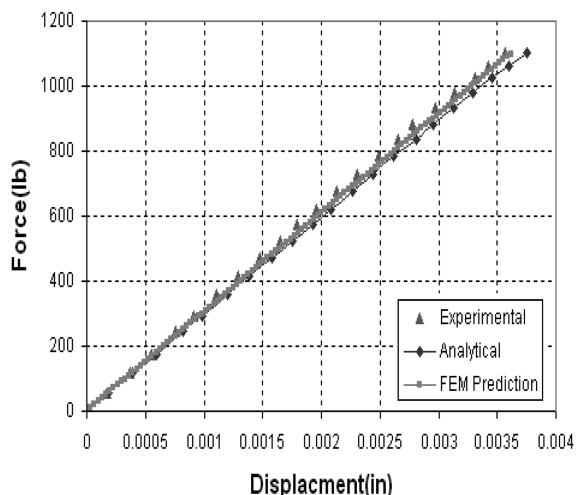


Fig. 8 Force vs. displacement for Al6061-T6 under monotonic tension and compression

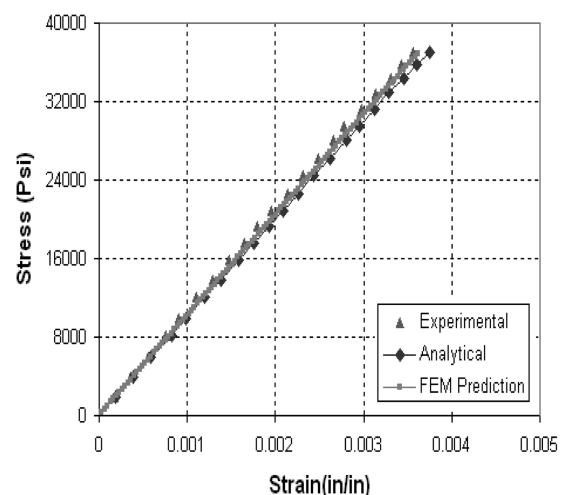


Fig. 9 True Stress vs. true strain for Al6061-T6 under monotonic tension and compression

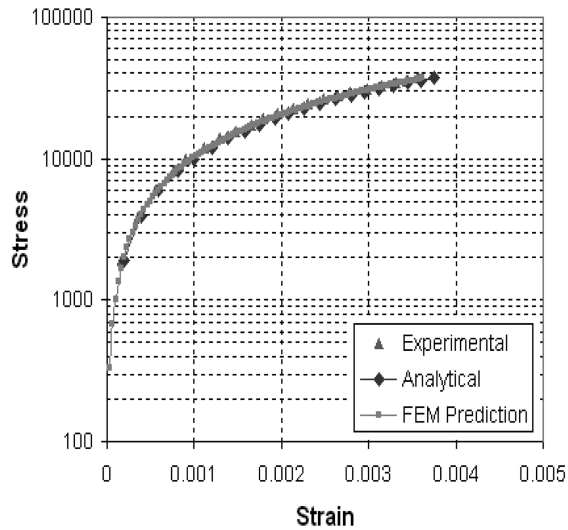


Fig. 10 Normalized data plot for Al6061-T6 under monotonic tension and compression

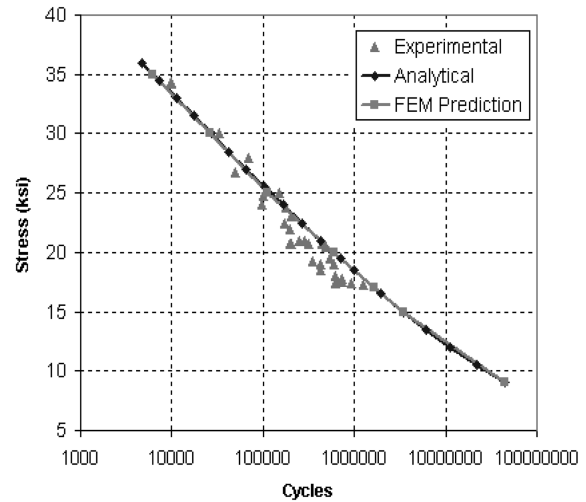


Fig. 11 Stress vs. no. of cycles for Al6061-T6 for completely reversible loading case

Table 2 Cyclic energy comparison for analytical solution and FEM prediction

Stress (Ksi)	Cyclic Energy (Analytical) (lb/in)/in ³ × 10 ³	Cyclic Energy(FEM) (lb/in)/in ³ × 10 ³	% Difference
35	8.52E+00	8.71E+00	2.2
30	1.99E+00	2.02E+00	1.4
25	4.41E-01	4.44E-01	0.7
20	8.98E-02	9.00E-02	0.1
15	1.57E-02	1.56E-02	0.3
9	1.18E-03	1.20E-03	1.4

Table 3 Number of cycle comparison between analytical solution and FEM prediction

Stress (Ksi)	Cycles (Analytical)	Cycles (FEM)	% Difference
35	6.28E+03	6.14E+03	2.2
30	2.69E+04	2.65E+04	1.4
25	1.21E+05	1.20E+05	0.7
20	5.96E+05	5.95E+05	0.1
15	3.42E+06	3.43E+06	0.3
9	4.52E+07	4.45E+07	1.4

Table 2 shows a comparison of cyclic energy for analytical results (Scott-Emuakpor *et al.* 2007) and FEM prediction. The percent difference between the two results is below 2.2%. This verifies a good match between results and also validates the new finite element.

Table 3 presents a comparison between number of cycles predicted in previous research (Scott-Emuakpor *et al.* 2007) and with new finite element.

Since there is a direct correlation between cyclic energy and cycles to failure, the maximum percent difference for assorted stress levels is also below 2.2 percent. This provides another indicator for a good agreement between the two methods.

This research deals with the elastic and plastic parts of Eqs. (1) and (2) separately and ignores any coupling between elastic and plastic strains. However, in the real world, this may not be the case. As it transpires, this coupling becomes stronger with the increasing stress in particular above the yield point. Therefore, a deviation of FEM prediction from the analytical data at higher stress levels is observed. The fatigue analysis is performed only below the yield point. Therefore, the level of applied stress remains low enough to cause any significant error due to coupling on the final results for number of cycles to failure. This is also evident from Figs. 8 and 9 that the difference between experimental data and FE prediction is very negligible. Therefore, to avoid the complexity of the computation, the coupling between elastic and plastic parts is ignored.

Ti6Al-4V material is also analyzed using new finite element and results are plotted in Fig. 12. From the experimental results of Fig. 12, it can be observed that an endurance limit phenomenon is present. Due to uncertainties in energy behavior near the endurance limit, the analysis is performed for stress levels above 60 Ksi. Nevertheless, the results show a good match between analytical solution and FEM prediction.

The cyclic loading case with mean stress effect is different from the completely reversible loading (Nicholas and Maxwell 2003). The calculation of cyclic energy in this case involves a different approach due to presence of mean stress and strain on the scale. When mean stress is included in a fatigue procedure, it dissipates residual energy and increases the plastic strain per cycle, thus reducing the amount of cycles required to fatigue a specimen. When evaluating the fully reversed tension/compression cyclic behavior, two assumptions were set in place. It is considered that a significant amount of strain damage is caused by plastic deformation, and the tensile cyclic curve (from zero applied stress to peak-to-peak stress) is a slight modification of the true strain equation,

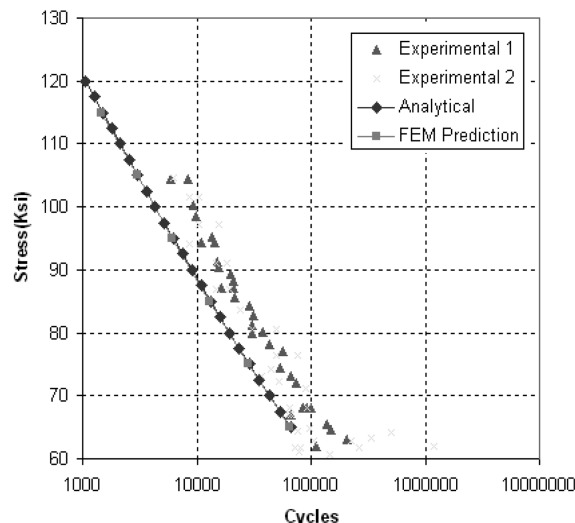


Fig. 12 Stress vs. no. of cycles for Ti6Al-4V for completely reversible loading case

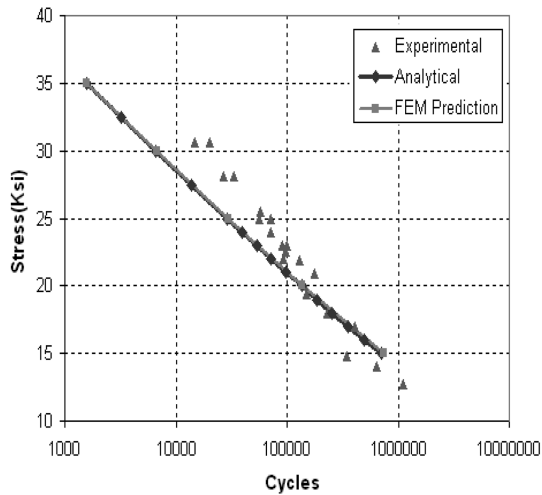


Fig. 13 S-N curve with 10 Ksi mean stress effect for Al6061-T6

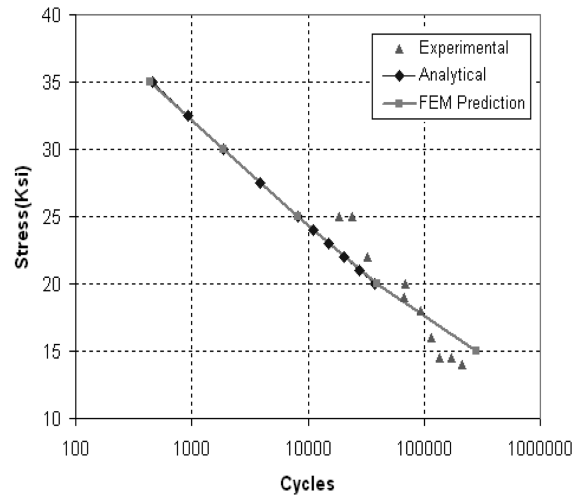


Fig. 14 S-N curve with 20 Ksi mean stress effect for Al6061-T6

which defines the stress-strain relation of a monotonic procedure (Scott-Emuakpor *et al.* 2007). In order to incorporate mean stress effect, both of these assumptions should still be in place. Meaning, each cycle, regardless of the mean stress value, should be plotted on the same axis and evaluated with the same cyclic tensile strain equation (Scott-Emuakpor *et al.* 2007) as the fully reversed cycle. However, unlike the fully-reversed case, it can not be assumed that the compressive behavior of the hysteresis loop (stress strain plot for one complete cycle) is identical to the tensile curve. Meaning, the curve from zero applied stress to peak-to-peak is not the same as the curve from peak-to-peak to zero. This assertion is proven by the experimental results, where the compressive curve was shown to be reasonably linear, thus providing a rather fair assumption for analytical characterization. As stated earlier, and illustrated in Fig. 7, the effect of the mean stress increases the amount of plastic deformation per cycle. This effect, as well as the residual mean strain energy, will reduce the fatigue life of materials with stress ratios greater than negative one.

The FE analysis is performed for Al6061-T6 with mean stress effect included. The results are plotted in Figs. 13 and 14 for 10 Ksi and 20 Ksi mean stress levels respectively. The FEM prediction curve follows the analytical results and experimental data closely.

5.2 Bending load analysis

Fig. 15 shows results for Al6061-T6 for completely reversible bending load. The FEM analysis is performed for number of elements ranging from 1 to 5. The results tend to converge to the analytical solution with increasing number of elements. The FEM results show a good agreement with analytical and experimental data (Scott-Emuakpor *et al.* 2007).

Table 4 provides a comparison of FEM prediction and analytical solution for a 5 element analysis. The results show a reasonable match which provides another indicator for an agreement between analytical (Scott-Emuakpor *et al.* 2007) and FEM predictions.

As stated earlier, the new bending element (K-Matrix) has the capability to predict different number of cycles for different elements in the structure subjected to varying stress. Figs. 16 and 17

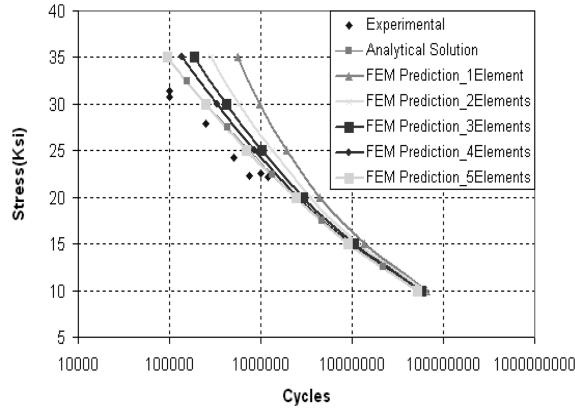


Fig. 15 Stress vs. no. of cycles for Al6061-T6 for completely reversible bending load

Table 4 Number of cycle comparison between analytical solution and FEM prediction (5 Elements) under bending loads

Stress (Ksi)	Cycles (Analytical)	Cycles (FEM)	% Difference
20	2.42E+06	2.340E+06	3.56
25	7.48E+05	7.220E+05	3.51
30	2.58E+05	2.500E+05	3.10
35	9.52E+04	9.551E+04	0.20

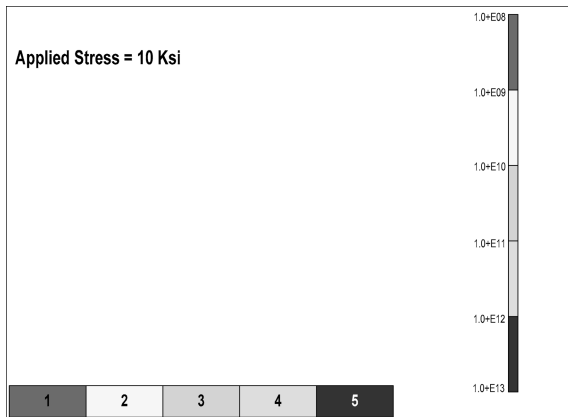


Fig. 16 No. of cycles for Al6061-T6 for completely reversible bending load (10 Ksi) – 5 element analysis

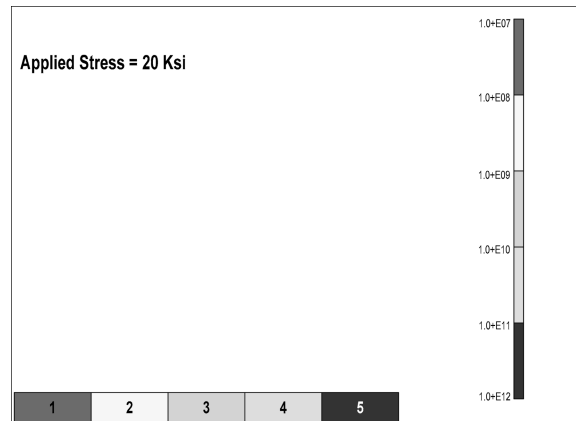


Fig. 17 No. of cycles for Al6061-T6 for completely reversible bending load (20 Ksi) – 5 element analysis

show 5 element cantilever beam analysis for 10 Ksi and 20 Ksi bending loads. The number of cycles is plotted using a colored contour plot where each color represents corresponding number of cycles in the element according to the scale. The scale is plotted from highest number of cycles,

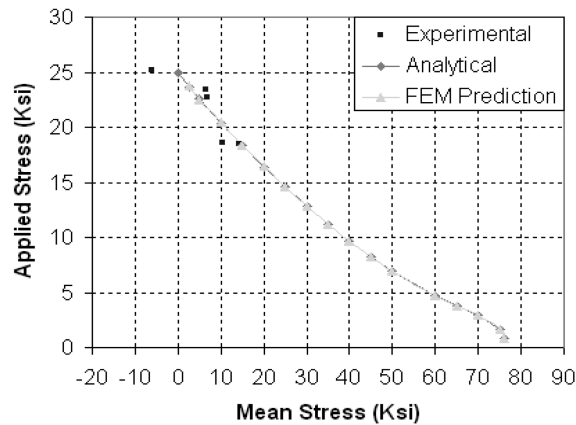


Fig. 18 Goodman diagram for Al6061-T6 with 5 element analyses

represented with blue color, to the lowest numbers represented with red color as shown in the Figs. Element 1 experiences the maximum stress, therefore, minimum number of cycles are predicted for this element. On the other hand, element 5 experiences the minimum stress, therefore, it can withstand maximum number of cycles in the beam.

Fig. 18 shows a Goodman diagram where applied stress is plotted vs. mean stress. The FEM analysis is performed with 5 element approximation. The results show a good match between analytical, experimental (Scott-Emuakpor *et al.* 2007) and FEM results.

6. Conclusions

The new finite elements (rod and beam) developed in this research provide a useful tool for fatigue life prediction in structural components like gas engine turbine blades. The accurate prediction of number of cycles with new axial and bending finite elements and a good match of results to experimental data and analytical results (Scott-Emuakpor *et al.* 2007) signifies that new finite elements provide sufficient estimation of number of cycles for axial and bending loads.

These new axial (rod) and bending (beam) elements are developed from a fatigue based constitutive law. The fact that these elements incorporate the fatigue mechanism in to analysis procedure differentiates these new developments from the existing finite element procedure. Furthermore, the new finite element method is much more useful due to the discrete nature of the finite element method. The new finite element for bending fatigue life prediction has the capability to predict varying number of cycles in the structural component experiencing variable stress at different locations. The colored plots can be obtained where each color signifies respective fatigue life for each element present at different locations in the structure.

Acknowledgements

The authors would like to thank the Honda of America (R&D) and Air force Research Lab (AFRL), Dayton, Ohio, USA for their financial support and encouragement of this research.

References

- Beretta, S. and Sala, G. (2005), "A model for fatigue strength of welded lap joints", *Fatigue Fract. Eng. Mater. Struct.*, **28**(1-2), 257-264.
- Desktop Engineering (DE), Fatigue Analysis Manual, <http://www.deskeng.com>
- Enomoto, N. (1955), "On fatigue tests under progressive stress", *Proc. ASTM*, **55**, 903-915.
- Feltner, C.E. and Morrow, J.D. (1960), "Micro plastic strain hysteresis energy as a criterion for fatigue failure", *Trans., ASME, J. Basic Eng.*, Paper No. 60-MET-2.
- Fermér, M. and Svensson, H. (2001), "Industrial experiences of FE-based fatigue life predictions of welded automotive structures", *Fatigue Fract. Eng. Mater. Struct.*, **24**(7), 489-500.
- George, T., Seidt, J., Shen, M.H.H., Cross, C. and Nicholas, T. (2004), "Development of a novel vibration-based fatigue testing methodology", *Int. J. Fatigue*, **26**(5), 477-486.
- George, T., Shen, M.H.H., Cross, C. and Nicholas, T. (2006), "A new multiaxial fatigue testing method for variable-amplitude loading and stress ratio", *J. Eng. Gas Turb. Power*, **128**, 857-864.
- George, T., Shen, M.H.H., Scott-Emuakpor, O., Cross, C., Nicholas, T. and Calcaterra, J. (2005), "Goodman diagram via vibration-based fatigue testing", *J. Eng. Mater. Technol.*, **127**(1), 58-64.
- Goodman, J. (1899), *Mechanics Applied to Engineering*, Longmans, Green and Co., London.
- Khurram, R.A. and Masud, A. (2006), "A multiscale/stabilized formulation of the incompressible navier-stokes equations for moving boundary flows and fluid structure interaction", *Comput. Mech.*, **38**, 4-5.
- Lee, H.J. and Song, J.H. (2005), "Finite-element analysis of fatigue crack closure under plane strain conditions: stabilization behavior and mesh size effect", *Fatigue Fract. Eng. Mater. Struct.*, **28**(3), 333-342.
- LMS Engineering Innovations, Fatigue Analysis Manual, <http://www.lmsintl.com>
- Mackaldener, M. and Olsson, M. (2001), "Interior fatigue fracture of gear teeth fatigue", *Fatigue Fract. Eng. Mater. Struct.*, **23**(4), 283-292.
- Masud, A. and Khurram, R.A. (2004), "A multiscale finite element method for the incompressible navier-stokes equations", *Comput. Meth. Appl. Mech. Eng.*, **193**, 21-22.
- MSC Software, Fatigue Analysis Manual, <http://www.mssoftware.com>
- Nicholas, T. (1999), "Critical issues in high cycles fatigue", *Int. J. Fatigue.*, **21**, 221-231.
- Nicholas, T. and Maxwell, D. (2003), "Mean stress effects on the high cycle fatigue limit stress in Ti-6Al-4V", *Fatigue Fract. Mech.*, ASTM STP 1417, **33**, 476-492, ASTM STP 1417.
- Papanikos, P. and Meguid, S.A. (1994), "Theoretical and experimental studies of fretting-initiated fatigue failure of aero engine compressor discs", *Fatigue Fract. Eng. Mater. Struct.*, **17**(5), 539-550.
- Papanikos, P., Tserpes, K.I. and Pantelakis, S.P. (2003), "Modeling of fatigue damage progression and life of CFRP laminates", *Fatigue Fract. Eng. Mater. Struct.*, **26**(1), 37-47.
- Park, S.J., Earmme, Y.Y. and Song, J.H. (1997), "Determination of the most appropriate mesh size for a 2-d finite element analysis of fatigue crack closure behavior", *Fatigue Fract. Eng. Mater. Struct.*, **20**(4), 533-545.
- Reddy, J.N. (1984), *An Introduction to the Finite Element Methods*, McGraw-Hill Book Company, New York.
- Reddy, J.N. (2004), *An Introduction to Non-Linear Finite Element Analysis*, Oxford University Press, New York.
- Ritchie, R.O., Yu, W., Blom, A.F. and Holm, D.K. (1987), "An analysis of crack tip shielding in aluminum Alloy 2124: A comparison of large, small, through-thickness and surface fatigue cracks", *Fatigue Fract. Eng. Mater. Struct.*, **10**(5), 343-362.
- Salvini, P., Cardecchia, E. and Emofonti, G. (1997), "A procedure for fatigue life prediction of spot welded joints", *Fatigue Fract. Eng. Mater. Struct.*, **20**(8), 1117-1128.
- Scott-Emuakpor, O. (2007), "Development of a novel energy based method for multiaxial fatigue strength assessment", The Ohio State University.
- Scott-Emuakpor, O., Shen, M.H.H., Cross, C., Calcaterra, J. and George, T. (2007), "Development of an improved high cycle fatigue criterion", *J. Eng. Gas Turb. Power*, **129**, 162-169.
- Shang, D.G. and Barkey, M.E. (2006), "Analysis of fatigue crack behavior based on dynamic response simulations and experiments for tensile-shear spot-welded joints", *Fatigue Fract. Eng. Mater. Struct.*, **29**(1), 23-30.

- Stowell, E. (1996), "A study of the energy criterion for fatigue", *Nucl. Eng. Des.*, **3**, 32-40.
- Sumi, Y., Mohri, M. and Kawamura, Y. (2005), "Computational prediction of fatigue crack paths in ship structural details", *Fatigue Fract. Eng. Mater. Struct.*, **28**(1-2), 107-115.